Journal of Robotics and Control (JRC)
Volume 3, Issue 2, March 2022
ISSN: 2715-5072 DOI: 10.18196/jrc.v3i2.13368

Backstepping-based Super-Twisting Sliding Mode Control for a Quadrotor Manipulator with Tiltable Rotors

Shilin Yi [1*], Keigo Watanabe [2], Isaku Nagai [3]
[1, 2, 3] Graduate School of Natural Science and Technology, Okayama University, Okayama 700-8530, Japan
[2] BAICIRS, Beijing Institute of Technology (BIT), Beijing, China
Email: [1] pwuq1uf4@s.okayama-u.ac.jp, [2] watanabe@sys.okayama-u.ac.jp, [3] in@sys.okayama-u.ac.jp
*Corresponding Author

***Abstract*—Designing a robust controller is very important in the control of outdoor unmanned aerial vehicles. This paper presents the design procedures and implementation of super-twisting sliding mode controller, which is a robust nonlinear controller. The robust controller is applied to an over-actuated quadrotor manipulator with four tiltable rotors. A serial manipulator with two links is mounted on the bottom of the quadrotor. The quadrotor possesses the property of decoupling its position and orientation. The main contribute of this paper is that a super-twisting sliding mode controller in vector form is designed and applied to the control of an over-actuated quadrotor manipulator. Another contribution of this paper is that the stability of the closed-loop system is proved by utilizing the Lyapunov stability theory. It is confirmed that the performance of the super-twisting sliding mode controller is superior to that of the conventional backstepping controller in terms of convergence rate and accuracy by simulations.**

Keywords—Super-twisting; Backstepping; Disturbance; Tiltable Rotors; Quadrotor Manipulator.

I. INTRODUCTION

Unmanned aerial vehicle manipulator (UAVM) is considered as a promising and potential aerial platform which can extend the tasks of conventional unmanned aerial vehicles (UAVs) from air [1]. UAVM is a combination of a UAV and a manipulator system [2]. In recent years, UAVMs were under the spotlight of numerous research groups. UAVMs shifted the application paradigms of UAVs from passive tasks like remote sensing, monitoring, aerial photography, reconnaissance [1], to active physical interacting tasks like grasping, transporting objects, infrastructure repair, industrial inspection, sensor installation and disaster response [3]–[8]. The needs of reducing time, cost, especially, the operations in high attitude workspaces, hazardous environments and locations where it is inaccessible for human beings lead to the appearance and advancement of UAVMs [9], [10]. A convenient way of building a UAVM is to attach a manipulator or several manipulators to a multirotor-type UAV [4].

However, the classical multirotor-based UAVMs inherit the under actuation properties of the UAVs, which means that the position and the orientation of the end-effector may be coupled [11]. One efficient method of overcoming the disadvantage is increasing the degrees of freedom (DOFs) of the manipulator or designing a manipulator with a unique topology [12]. In [13], a quadrotor in coaxial rotor configuration with a 7-DOF manipulator was proposed to increase the manipulation capability. Another efficient method of overcoming the disadvantage of under actuation is designing fully-actuated or over-actuated UAVMs by tilting the rotors of the UAVs. The hexarotor with 6 fixed-tilt rotors gains the property of full actuation without the need of additional hardware [14]. In [15], Ryll et al. presented a fully-actuated UAVM, whose end-effector were fixedly mounted on a hexarotor with tilted rotors. The UAVM was demonstrated to be capable of exerting full wrench in physically interactive tasks. In [16], a fully-actuated UAVM with a multi-link robotic arm installed on the top of a fully-actuated hexarotor was designed for infrastructure contact inspection. In [17], Ryll et al. presented a novel hexarotor concept that can smoothly transform its configuration from under actuation to full actuation by adding only one motor that tilts all propellers simultaneously. As a significant property of fully-actuated or over-actuated UAVMs, these UAVMs can achieve decoupled control of its position and orientation. Therefore, fully-actuated or over-actuated UAVMs are important aerial platforms in physically interactive tasks [8], [18].

A UAVM can be considered as a tree-like floating multi-body system, whose dynamical model is highly nonlinear, which makes the control of a UAVM be a challenging problem. Additionally, external wind disturbances may destabilize the UAVM in the air [8], [19], [20]. In the past years, many kinds of nonlinear control strategy have been proposed to address these problems. In [21], Suarez et al. applied virtual impedance control to a conventional hexarotor with an anthropomorphic, compliant and lightweight dual arm. Ruggiero et al. [2] proposed a multilayer architecture to control a coaxial quadrotor with a 6-DOF manipulator driven by servo motors. Ali and Li [22] proposed a model-based adaptive controller to be applied to a quadrotor equipped with a gripper. Jiao et al. [23] proposed an adaptive super-twisting sliding mode observer to estimate the external wind disturbances for high-precision attitude control of a quadrotor manipulator.

In the field of robust control, sliding mode control is a famous robust control method. As a robust controller, a sliding mode controller is robust with respect to external disturbances and internal parameter uncertainties [24], [25].

However, the cost of achieving the robustness of the sliding mode controller is the happening of chattering phenomenon in the control inputs, which is an undesirable oscillation with finite frequency and amplitude [26], [27]. The advent of high order sliding mode controllers is to address the chattering problem [28]. As a second order sliding mode controller [29], [30], super-twisting sliding mode controller proposed by Levant [31] is capable of converging to the origin in finite time and attenuating the chattering phenomenon without the need to calculating the derivative of sliding variable [32], [33].

To the best of the authors' knowledge, this is the first time that a super-twisting sliding mode controller in vector form is proposed to be applied to the quadrotor manipulator with four tiltable rotors. Also, the stability and robustness of the proposed controller is proved based on the Lyapunov stability theory. In addition to the theoretical proof of the robustness of the proposed controller, the effectiveness of the proposed controller is validated by simulations with comparisons with the classical backstepping controller.

In Section II, the dynamical model of the quadrotor manipulator is described. The designing procedures of the super-twisting sliding mode controller are explained in Section III. In Section IV the performance of the super-twisting sliding mode controller is validated by comparing it with that of the conventional backstepping controller. Finally, the conclusion of this paper is summarized in Section V.

II. MODELING OF THE QUADROTOR MANIPULATOR

In this research, the quadrotor manipulator model proposed in [34] is adopted. The mechanical structure of the quadrotor manipulator consists of two parts. One part is a quadrotor with four tiltable rotors and the other part is a manipulator consisting of 2 links. The quadrotor manipulator with four tiltable rotors is capable of changing the thrust directions of the rotors, which makes the quadrotor manipulator possess the property of controlling its position and orientation separately. The overview of the quadrotor manipulator and the definition of coordinate systems are shown in Fig. 1.

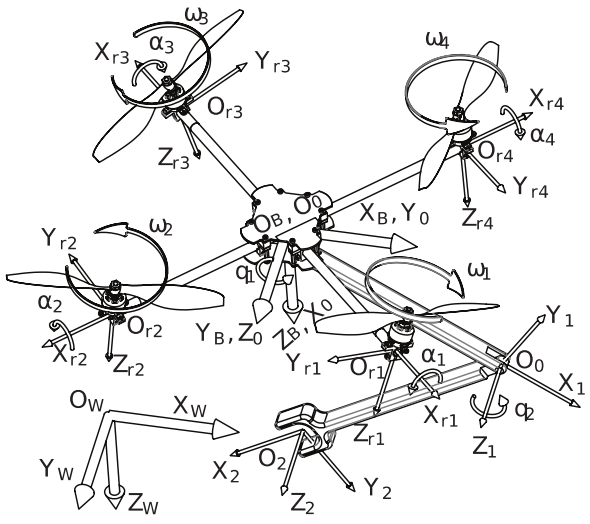

Fig. 1. Overview and coordinates of the quadrotor manipulator with four tiltable rotors

As shown in Fig. 1, $\mathcal{F}_{\mathrm{W}}$: $\{\mathrm{X_W}, \mathrm{Y_W}, \mathrm{Z_W}\}$ denotes the world inertial coordinate and $\mathcal{F}_{\mathrm{B}}$: $\{\mathrm{X_B}, \mathrm{Y_B}, \mathrm{Z_B}\}$ is the body-fixed coordinate which is attached to the geometrical center of the quadrotor body. $\mathcal{F}_{\mathrm{r}_i}$: $\{\mathrm{X}_{\mathrm{r}_i}, \mathrm{Y}_{\mathrm{r}_i}, \mathrm{Z}_{\mathrm{r}_i}\}$, $i = 1, \ldots, 4$ are defined as the coordinates attached to each rotor. As for the coordinates of the manipulator, $\mathcal{F}_0$: $\{\mathrm{X_0}, \mathrm{Y_0}, \mathrm{Z_0}\}$ represents the base coordinate of the manipulator with its origin located at the same location as that of $\mathcal{F}_{\mathrm{B}}$, but with different directions of axes. $\mathcal{F}_1$: $\{\mathrm{X_1}, \mathrm{Y_1}, \mathrm{Z_1}\}$ and $\mathcal{F}_2$: $\{\mathrm{X_2}, \mathrm{Y_2}, \mathrm{Z_2}\}$ are attached to the end of the link 1 and the link 2, respectively.

A. Mathematical model

The details of deriving the dynamic model of the quadrotor manipulator are described in [34]. For easy comprehension of this paper, the dynamic model of the quadrotor manipulator is rewritten here. Following the Euler-Lagrange approach, the dynamic model of the quadrotor manipulator is derived by treating the quadrotor part and the manipulator part as a unique system. Then, the dynamical equation of the quadrotor manipulator can be written as

$$\begin{aligned}\boldsymbol{M}(\boldsymbol{\xi}_{\mathrm{Q}})\ddot{\boldsymbol{\xi}}_{\mathrm{QM}} + \boldsymbol{V}(\boldsymbol{\xi}_{\mathrm{Q}}, \dot{\boldsymbol{\xi}}_{\mathrm{QM}})\dot{\boldsymbol{\xi}}_{\mathrm{QM}} + \boldsymbol{G}(\boldsymbol{\xi}_{\mathrm{Q}}) \\ = \boldsymbol{F}_{\mathrm{QM}} + \boldsymbol{F}_{\mathrm{ext}}\end{aligned} \tag{1}$$

where

$$\boldsymbol{\xi}_{\mathrm{QM}} \triangleq [x_B^W \quad y_B^W \quad z_B^W \quad \phi \quad \theta \quad \psi \quad q_1 \quad q_2]^{\mathrm{T}} \tag{2}$$

which is the generalized coordinates of the quadrotor manipulator, $[x_B^W \quad y_B^W \quad z_B^W]^{\mathrm{T}}$ represents the position of the quadrotor in $\mathcal{F}_{\mathrm{W}}$, $[\phi \quad \theta \quad \psi]^{\mathrm{T}}$ is the orientation of the quadrotor expressed in Euler angles, $[q_1 \quad q_2]^{\mathrm{T}}$ represents joint angles of the manipulator, $\boldsymbol{M}(\boldsymbol{\xi}_{\mathrm{QM}}) \in \mathbb{R}^{8\times 8}$ denotes a positive definite inertial matrix, $\boldsymbol{V}(\boldsymbol{\xi}_{\mathrm{Q}}, \dot{\boldsymbol{\xi}}_{\mathrm{QM}}) \in \mathbb{R}^{8\times 8}$ denotes the Coriolis/centripetal matrix, $\boldsymbol{G}(\boldsymbol{\xi}_{\mathrm{Q}}) \in \mathbb{R}^8$ is the gravity term and $\boldsymbol{F}_{\mathrm{ext}}$ represents the external disturbances.

$\boldsymbol{F}_{\mathrm{QM}}$ is the generalized forces exerted on the quadrotor manipulator, which can be expressed by

$$\boldsymbol{F}_{\mathrm{QM}} = \underbrace{\begin{bmatrix} \boldsymbol{R}_B^W & \boldsymbol{0} & \boldsymbol{0} \\ \boldsymbol{0} & \boldsymbol{I}_{3\times 3} & \boldsymbol{0} \\ \boldsymbol{0} & \boldsymbol{0} & \boldsymbol{I}_{2\times 2} \end{bmatrix}}_{\boldsymbol{R}(\boldsymbol{\xi}_{\mathrm{QM}})} \begin{bmatrix} \boldsymbol{F}_{\mathrm{Q}} \\ \boldsymbol{\tau}_{\mathrm{link}} \end{bmatrix} \tag{3}$$

where $\boldsymbol{R}(\boldsymbol{\xi}_{\mathrm{QM}})$ is a square matrix that transforms the wrench exerted on the quadrotor and the torques exerted on the manipulator to the generalized coordinate $\boldsymbol{\xi}_{\mathrm{QM}}$, $\boldsymbol{R}_B^W$ is the rotation matrix that represents the orientation from $\mathcal{F}_{\mathrm{B}}$ to $\mathcal{F}_{\mathrm{W}}$ and $\boldsymbol{\tau}_{\mathrm{link}}^{\mathrm{T}} = [\tau_1 \quad \tau_2]$ is the torques exerted on the manipulator.

$\boldsymbol{F}_{\mathrm{Q}} \in \mathbb{R}^6$ is denoted as the wrench exerted on the quadrotor and $\boldsymbol{F}_{\mathrm{Q}}$ can be calculated as

$$\boldsymbol{F}_{\mathrm{Q}} = \boldsymbol{A}_{\mathrm{c}}\boldsymbol{F}_{\omega} \tag{4}$$

$$A_{\mathrm{c}}=\begin{bmatrix}-\sigma_2 & 0 & -\sigma_2 & 0 & \sigma_2 & 0 & \sigma_2 & 0\\ \sigma_2 & 0 & -\sigma_2 & 0 & -\sigma_2 & 0 & \sigma_2 & 0\\ 0 & -K_{\mathrm{f}} & 0 & -K_{\mathrm{f}} & 0 & -K_{\mathrm{f}} & 0 & -K_{\mathrm{f}}\\ -\sigma_3 & -\sigma_1 & \sigma_3 & -\sigma_1 & \sigma_3 & \sigma_1 & -\sigma_3 & \sigma_1\\ \sigma_3 & \sigma_1 & \sigma_3 & -\sigma_1 & -\sigma_3 & -\sigma_1 & -\sigma_3 & \sigma_1\\ LK_{\mathrm{f}} & -K_{\mathrm{d}} & LK_{\mathrm{f}} & K_{\mathrm{d}} & LK_{\mathrm{f}} & -K_{\mathrm{d}} & LK_{\mathrm{f}} & K_{\mathrm{d}}\end{bmatrix} \quad (5)$$

where

$$\sigma_1=\sqrt{2}\mathrm{L}K_{\mathrm{f}}/2,\ \sigma_2=\sqrt{2}K_{\mathrm{f}}/2,\ \sigma_3=\sqrt{2}K_{\mathrm{d}}/2, \quad (6)$$

and $\boldsymbol{A}_c$ is often named an allocation matrix, which is determined by the number and position of each rotor with respect to the quadrotor. K_{f} represents the lift force coefficient of each propeller, K_{d} represents the drag force coefficient of each propeller, L stands for the arm length of the quadrotor and $\boldsymbol{F}_\omega$ is a vector defined as below:

$$\boldsymbol{F}_\omega = \begin{bmatrix}\omega_1^2\mathrm{s}_{\alpha_1} & \omega_1^2\mathrm{c}_{\alpha_1} & \omega_2^2\mathrm{s}_{\alpha_2} & \omega_2^2\mathrm{c}_{\alpha_2}\\ \omega_3^2\mathrm{s}_{\alpha_3} & \omega_3^2\mathrm{c}_{\alpha_3} & \omega_4^2\mathrm{s}_{\alpha_4} & \omega_4^2\mathrm{c}_{\alpha_4}\end{bmatrix}^{\mathrm{T}}, \quad (7)$$

where c. and s. stand for trigonometric functions $\cos(\cdot)$ and $\sin(\cdot)$. α_i is denoted as the tilting angle of each rotor and ω_i is the angular velocity of each rotor.

B. Inverse kinematics

For convenience, link 2 of the manipulator is referred as the end-effector of the manipulator. $\boldsymbol{\xi}_{\mathrm{e}} \in \mathbb{R}^6$ is denoted as the coordinate of the tip of the end-effector in the task space.

From the viewpoint of controlling, it is critical to express $\boldsymbol{\xi}_{\mathrm{QM}}$ in terms of $\boldsymbol{\xi}_{\mathrm{e}}$. However, an analytical solution of $\boldsymbol{\xi}_{\mathrm{QM}}$ cannot be obtained because of the redundancy of the quadrotor manipulator. Therefore, a numerical approach called the Levenberg-Marquardt method is proposed to be applied to the quadrotor manipulator. In addition, this method behaves well in the neighborhood of singularities [35]. $\boldsymbol{J}_{\boldsymbol{\eta}} \in \mathbb{R}^{6\times 8}$ is the analytical Jacobian matrix of the end-effector and the forward kinematics of the end-effector is given by

$$\dot{\boldsymbol{\xi}}_{\mathrm{e}} = \boldsymbol{J}_{\boldsymbol{\eta}_{\mathrm{e}}}\dot{\boldsymbol{\xi}}_{\mathrm{QM}} \quad (8)$$

$\boldsymbol{\xi}_{\mathrm{d}}$ is denoted as the desired trajectory of the end-effector and $\boldsymbol{\varepsilon} = \boldsymbol{\xi}_{\mathrm{d}} - \boldsymbol{\xi}_{\mathrm{e}}$ is called the calculating trajectory error. Then, the inverse kinematics problem can be solved by

$$\Delta\boldsymbol{\xi}_{\mathrm{QM}} = \boldsymbol{J}_{\boldsymbol{\eta}_{\mathrm{e}}}^{\mathrm{T}}\left(\boldsymbol{J}_{\boldsymbol{\eta}_{\mathrm{e}}}\boldsymbol{J}_{\boldsymbol{\eta}_{\mathrm{e}}}^{\mathrm{T}} + \lambda^2\boldsymbol{I}_{6\times 6}\right)^{-1}\boldsymbol{\varepsilon} \quad (9)$$

where $\Delta\boldsymbol{\xi}_{\mathrm{QM}}$ is denoted as the variation of $\boldsymbol{\xi}_{\mathrm{QM}}$ and λ is a non-zero damping constant. It is found that Eq. (9) is numerically stable and well-behaved near singularities when λ is chosen as positive constant 1.

III. CONTROLLER DESIGN

Generally, the super-twisting sliding mode controller can be separated into two parts. One is the equivalent control part and the other one is the switching control part [36]. In this section, a super-twisting sliding mode control method is proposed to be applied to the quadrotor manipulator with four tiltable rotors. The stability and robustness of the proposed super-twisting sliding mode controller is proved by using the backstepping control method and Lyapunov stability theory.

Firstly, the state variables are introduced and defined as below,

$$\boldsymbol{x}_1 = \boldsymbol{\xi}_{\mathrm{QM}}, \boldsymbol{x}_2 = \dot{\boldsymbol{x}}_1, \boldsymbol{X} \triangleq \begin{bmatrix}\boldsymbol{x}_1\\ \boldsymbol{x}_2\end{bmatrix} \quad (10)$$

Then, Eq. (1) can be written as the state-space expression as below:

$$\begin{aligned}\dot{\boldsymbol{x}}_1 &= \boldsymbol{x}_2\\ \dot{\boldsymbol{x}}_2 &= \boldsymbol{f}(\boldsymbol{x}_1,\boldsymbol{x}_2) + \boldsymbol{g}(\boldsymbol{x}_1)\left(\boldsymbol{F}_{\mathrm{QM}} + \boldsymbol{F}_{\mathrm{ext}}\right)\end{aligned} \quad (11)$$

In order to simplify the model of external disturbances, the wind forces $\boldsymbol{F}_{\mathrm{wind}}$ are considered to be exerted on the center of mass of the quadrotor manipulator. Moreover, the torques generated by the wind forces and external disturbances exerted on the links of the manipulator can be ignored. Thus, $\boldsymbol{F}_{\mathrm{ext}} \in \mathbb{R}^8$ can be defined as

$$\boldsymbol{F}_{\mathrm{ext}} = \begin{bmatrix}\boldsymbol{F}_{\mathrm{wind}}\\ \boldsymbol{0}\end{bmatrix} \quad (12)$$

A. Design of backstepping-based super-twisting sliding mode controller

The objective of this section is to design a super-twisting sliding mode controller. Firstly, $\boldsymbol{x}_{1\mathrm{d}}$ is introduced to denote the reference of $\boldsymbol{x}_1$. Then, the tracking error can be defined as $\boldsymbol{e}_1$, which is given by

$$\boldsymbol{e}_1 = \boldsymbol{x}_{1\mathrm{d}} - \boldsymbol{x}_1 \quad (13)$$

The derivative of $\boldsymbol{e}_1$is denoted as $\boldsymbol{e}_2$, which is calculated as

$$\boldsymbol{e}_2 = \dot{\boldsymbol{e}}_1 = \dot{\boldsymbol{x}}_{1\mathrm{d}} - \dot{\boldsymbol{x}}_1 = \dot{\boldsymbol{x}}_{1\mathrm{d}} - \boldsymbol{x}_2 \quad (14)$$

To make sure the stability of the system (11), the first Lyapunov function candidate for the backstepping control is chosen as

$$V_1 = \frac{1}{2}\boldsymbol{e}_1^{\mathrm{T}}\boldsymbol{e}_1 \quad (15)$$

The derivative of the Lyapunov function V_1 with respect to time can be calculated as

$$\begin{aligned}\dot{V}_1 &= \boldsymbol{e}_1^{\mathrm{T}}\dot{\boldsymbol{e}}_1\\ &= \boldsymbol{e}_1^{\mathrm{T}}\boldsymbol{e}_2\\ &= -\boldsymbol{e}_1^{\mathrm{T}}\boldsymbol{K}_1\boldsymbol{e}_1 + \boldsymbol{e}_1^{\mathrm{T}}(\boldsymbol{K}_1\boldsymbol{e}_1 + \boldsymbol{e}_2)\end{aligned} \quad (16)$$

where $\boldsymbol{K}_1$ is positive definite diagonal matrix. According to the form of right-hand side of (16), a sliding hyperplane $\boldsymbol{S}$ is introduced such as

$$\boldsymbol{S} = \boldsymbol{K}_1\boldsymbol{e}_1 + \boldsymbol{e}_2 \quad (17)$$

Then, the derivative of $\boldsymbol{S}$ can be calculated as below:

$$\begin{aligned}\dot{\boldsymbol{S}} = &\ \boldsymbol{K}_1\dot{\boldsymbol{e}}_1 + \dot{\boldsymbol{e}}_2 \\ = &\ \boldsymbol{K}_1\boldsymbol{e}_2 + (\ddot{\boldsymbol{x}}_{1\mathrm{d}} - \dot{\boldsymbol{x}}_2) \\ = &\ \boldsymbol{K}_1\boldsymbol{e}_2 + [\ddot{\boldsymbol{x}}_{1\mathrm{d}} - (\boldsymbol{f}(\boldsymbol{x}_1,\boldsymbol{x}_2) \\ &+\boldsymbol{g}(\boldsymbol{x}_1)(\boldsymbol{F}_{\mathrm{QM}} + \boldsymbol{F}_{\mathrm{ext}}))]\end{aligned} \tag{18}$$

The second Lyapunov function candidate for the backstepping control is chosen as

$$V_2 = V_1 + \frac{1}{2}\boldsymbol{S}^{\mathrm{T}}\boldsymbol{S} \tag{19}$$

Next, the derivative of V_2 with respect to time can be calculated as below:

$$\begin{aligned}\dot{V}_2 = &\ \dot{V}_1 + \boldsymbol{S}^{\mathrm{T}}\dot{\boldsymbol{S}} \\ = &\ -\boldsymbol{e}_1^{\mathrm{T}}\boldsymbol{K}_1\boldsymbol{e}_1 + \boldsymbol{e}_1^{\mathrm{T}}\boldsymbol{S} + \boldsymbol{S}^{\mathrm{T}}\dot{\boldsymbol{S}} \\ = &\ -\boldsymbol{e}_1^{\mathrm{T}}\boldsymbol{K}_1\boldsymbol{e}_1 + \boldsymbol{e}_1^{\mathrm{T}}\boldsymbol{S} + \boldsymbol{S}^{\mathrm{T}}(\boldsymbol{K}_1\boldsymbol{e}_2 \\ &+\left[\ddot{\boldsymbol{x}}_{1\mathrm{d}} - \left(\boldsymbol{f}(\boldsymbol{x}_1,\boldsymbol{x}_2) + \boldsymbol{g}(\boldsymbol{x}_1)(\boldsymbol{F}_{\mathrm{QM}} + \boldsymbol{F}_{\mathrm{ext}})\right)\right])\end{aligned} \tag{20}$$

If $\boldsymbol{S} = \dot{\boldsymbol{S}} = \boldsymbol{0}$ is satisfied, Eq. (20) can be assured such that $\dot{V}_2 \leq 0$. The generalized force input $\boldsymbol{F}_{\mathrm{QM}}$ can be separated into two parts:

$$\boldsymbol{F}_{\mathrm{QM}} = \boldsymbol{F}_{\mathrm{QM}}^0 + \boldsymbol{F}_{\mathrm{QM}}^1, \tag{21}$$

where $\boldsymbol{F}_{\mathrm{QM}}^0$ is called the equivalent input and $\boldsymbol{F}_{\mathrm{QM}}^1$ is called the switching input for suppressing the influence of $\boldsymbol{F}_{\mathrm{ext}}$. Then, in order to force the condition $\boldsymbol{S} = \dot{\boldsymbol{S}} = \boldsymbol{0}$ to be satisfied, the equivalent input $\boldsymbol{F}_{\mathrm{QM}}^0$ is designed as

$$\boldsymbol{F}_{\mathrm{QM}}^0 = \boldsymbol{g}^{-1}(\boldsymbol{x}_1)\left(\boldsymbol{K}_1\boldsymbol{e}_2 + \left(\ddot{\boldsymbol{x}}_{1\mathrm{d}} - \boldsymbol{f}(\boldsymbol{x}_1,\boldsymbol{x}_2)\right)\right) \tag{22}$$

Substituting Eq. (22) into Eq. (18), $\dot{\boldsymbol{S}}$ can be simplified as

$$\dot{\boldsymbol{S}} = -\boldsymbol{g}(\boldsymbol{x}_1)\left(\boldsymbol{F}_{\mathrm{QM}}^1 + \boldsymbol{F}_{\mathrm{ext}}\right) \tag{23}$$

For convenience, a disturbance vector $\boldsymbol{\Xi}$ is introduced which is defined as below:

$$\boldsymbol{\Xi} = -\boldsymbol{g}(\boldsymbol{x}_1)\boldsymbol{F}_{\mathrm{ext}} \tag{24}$$

It is assumed that $\| \dot{\boldsymbol{\Xi}} \| < d$, where $d \in \mathbb{R}^+$ is a positive scalar. Substituting Eq. (24) into Eq. (23), it is obtained that

$$\dot{\boldsymbol{S}} = -\boldsymbol{g}(\boldsymbol{x}_1)\boldsymbol{F}_{\mathrm{QM}}^1 + \boldsymbol{\Xi} \tag{25}$$

According to the super-twisting sliding mode control law [37], [38], $\boldsymbol{F}_{\mathrm{QM}}^1$ is designed as

$$\boldsymbol{F}_{\mathrm{QM}}^1 = \boldsymbol{g}^{-1}(\boldsymbol{x}_1)\left(\rho_1\frac{\boldsymbol{S}}{\| \boldsymbol{S} \|^{1/2}} + \rho_2\int_0^\tau \frac{\boldsymbol{S}}{\| \boldsymbol{S} \|}\mathrm{d}t\right), \tag{26}$$

where ρ_1 and ρ_2 are positive scalars and satisfy the following condition:

$$\rho_1 > \sqrt{2\rho_2},\ \rho_2 > 4d. \tag{27}$$

Substituting Eq. (26) into Eq. (25), the closed-loop system of $\boldsymbol{S}$ can rewritten as

$$\begin{aligned}\dot{\boldsymbol{S}} &= -\rho_1\frac{\boldsymbol{S}}{\| \boldsymbol{S} \|^{1/2}} + \boldsymbol{Z} \\ \dot{\boldsymbol{Z}} &= -\rho_2\frac{\boldsymbol{S}}{\| \boldsymbol{S} \|} + \dot{\boldsymbol{\Xi}}\end{aligned} \tag{28}$$

It can be proved that the dynamic system of $\boldsymbol{S}$ expressed in Eq. (28) converges to the origin in finite time when the condition given in Eq. (27) is satisfied. A Lyapunov function candidate is considered as below

$$V(\boldsymbol{S},\boldsymbol{Z}) = 2\rho_2\| \boldsymbol{S} \| + \frac{1}{2}\left(\| \boldsymbol{Z} \|^2 + \left\|\rho_1\frac{\boldsymbol{S}}{\| \boldsymbol{S} \|^{1/2}} - \boldsymbol{Z}\right\|^2\right) \tag{29}$$

which is continuous and differentiable at any point except $\boldsymbol{S} = \boldsymbol{0}$. It can also be verified that $V(\boldsymbol{S},\boldsymbol{Z})$ is positive definite and radially unbounded. According to the conclusion in [37], [38], the time derivative of $V(\boldsymbol{S},\boldsymbol{Z})$ can be proved to be negative definite. Then, it can be concluded that the dynamic system (28) converges to the equilibrium point $(\boldsymbol{S},\boldsymbol{Z}) = \boldsymbol{0}$ in finite time. Substituting $\boldsymbol{S} = \boldsymbol{Z} = \boldsymbol{0}$ into Eq. (28), it can be derived that $\dot{\boldsymbol{S}} = \boldsymbol{0}$. Finally, the condition $\boldsymbol{S} = \dot{\boldsymbol{S}} = \boldsymbol{0}$ is proved and $\dot{V}_2 \leq 0$ is assured in Eq. (20). According to the analysis in [37], the influence of $\dot{\boldsymbol{\Xi}}$ in Eq. (28) can still be suppressed when the condition (27) is further relaxed to

$$\rho_1 > \sqrt{2\rho_2},\ \rho_2 > d. \tag{33}$$

Therefore, it is proved that the backstepping-based super-twisting sliding mode controller (BSTSMC) proposed in this paper is able to converge to the reference in finite time despite of external disturbance.

B. Control allocation

Control allocation is the problem of determining the input of each rotor. In other words, the angular velocity of each rotor ω_i and the tilting angle of each rotor α_i should be solved, when $\boldsymbol{F}_{\mathrm{QM}}$ is known. Applying the control law Eq. (21), $\boldsymbol{F}_{\mathrm{Q}}$ can be obtained from Eq. (3). Based on the relation expressed in Eq. (4), the vector $\boldsymbol{F}_{\omega}$ can be derived. Since $\boldsymbol{A}_{\mathrm{c}}$ is not a square matrix, the solution of Eq. (4) cannot be decided uniquely. Therefore, $\boldsymbol{F}_{\omega}$ is solved by multiplying a pseudo-inverse of $\boldsymbol{A}_{\mathrm{c}}$ to the left side of Eq. (4), such as

$$\boldsymbol{F}_{\omega} = \boldsymbol{A}_{\mathrm{c}}^{\dagger}\boldsymbol{F}_{\mathrm{Q}}, \tag{34}$$

where $\boldsymbol{A}_c^{\dagger}$ is the pseudo-inverse matrix of $\boldsymbol{A}_c$. By exploiting the form of Eq. (7) and the characteristics of trigonometric functions, it is obtained for $i = 1, \ldots, 4$ that

$$\omega_i^2 = \sqrt{\boldsymbol{F}_{\omega}^2(2i-1) + \boldsymbol{F}_{\omega}^2(2i)} \tag{35}$$

$$\alpha_i = \mathrm{atan2}(\boldsymbol{F}_{\omega}^2(2i-1), \boldsymbol{F}_{\omega}^2(2i)) \tag{36}$$

TABLE I. PHYSICAL PARAMETERS OF THE QUADROTOR MANIPULATOR

Definition	Symbol	Value
Mass of the quadrotor	m_{B}	1.2 kg
Arm length of the quadrotor	L	0.25 m
Inertial moment of the quadrotor around the X-axis of $\mathcal{F}_{\mathrm{B}}$	$I_{\mathrm{B,xx}}$	0.0177 kg m^2
Inertial moment of the quadrotor around the Y-axis of $\mathcal{F}_{\mathrm{B}}$	$I_{\mathrm{B,yy}}$	0.0177 kg m^2
Inertial moment of the quadrotor around the Z-axis of $\mathcal{F}_{\mathrm{B}}$	$I_{\mathrm{B,zz}}$	0.0181 kg m^2
Mass of link 1 of the manipulator	m_1	0.210 kg
Length of link 1 of the manipulator	L_1	0.2 m
Mass of link 2 of the manipulator	m_2	0.255 kg
Length of link 2 of the manipulator	L_2	0.2 kg m^2
Inertial moment of link 1 around the X-axis of $\mathcal{F}_1$	$I_{1,\mathrm{xx}}$	1.430×10^{-5} kg m^2
Inertial moment of link 1 around the Y-axis of $\mathcal{F}_1$	$I_{1,\mathrm{yy}}$	1.505×10^{-3} kg m^2
Inertial moment of link 1 around the Z-axis of $\mathcal{F}_1$	$I_{1,\mathrm{zz}}$	1.505×10^{-3} kg m^2
Inertial moment of link 2 around the X-axis of $\mathcal{F}_2$	$I_{2,\mathrm{xx}}$	4.745×10^{-5} kg m^2
Inertial moment of link 2 around the Y-axis of $\mathcal{F}_2$	$I_{2,\mathrm{yy}}$	2.150×10^{-3} kg m^2
Inertial moment of link 2 around the Z-axis of $\mathcal{F}_2$	$I_{2,\mathrm{zz}}$	2.150×10^{-3} kg m^2
Lift force coefficient of the propellers	K_{f}	1.788×10^{-5} N s^2/rad^2
Drag force coefficient of the propellers	K_{d}	4.136×10^{-7}Nms^2/rad^2

IV. SIMULATION

In order to validate the effectiveness of the backstepping-based super-twisting sliding mode controller proposed in Sect. III, two classes of simulations of stabilization problem and trajectory tracking problem are conducted, where the sampling period is set to 0.001 s.

The physical parameters of quadrotor manipulator are organized in Table I. When it comes to the control of the quadrotor manipulator, external wind disturbances are inevitable. The quadrotor manipulator may deviate from the desired trajectory or even crash in the presence of external wind disturbances [23]. In this research, the following deterministic wind disturbance is adopted.

$$\boldsymbol{F}_{\mathrm{wind}} = \begin{bmatrix} 1.5\sin(4\pi t) + 1.5\cos(4\pi t) \\ 0.8\sin(4\pi t) + 0.8\cos(4\pi t) \\ 0.5\sin(4\pi t) + 0.5\cos(4\pi t) \end{bmatrix} \tag{37}$$

In order to show the effectiveness of the BSTSMC, a backstepping controller (BC) is introduced for comparison and the control law is given as

$$\begin{aligned} \boldsymbol{F}_{\mathrm{QM}} = \boldsymbol{g}^{-1}(\boldsymbol{x}_1)(\boldsymbol{e}_1 + \boldsymbol{K}_1\boldsymbol{e}_2 + \boldsymbol{K}_2\boldsymbol{S} \\ +(\ddot{\boldsymbol{x}}_{1\mathrm{d}} - \boldsymbol{f}(\boldsymbol{x}_1, \boldsymbol{x}_2)) \end{aligned} \tag{38}$$

where $\boldsymbol{K}_2$ is positive definite diagonal matrix.

It is estimated that $\| \dot{\Xi} \| < 80$ in this simulation. Based on the condition (33), ρ_2 is chosen to be 100 and ρ_1 is chosen to be 14.5. For easy comparison, the gain matrices $\boldsymbol{K}_1$ of both the BSTMC and the BC are designed to be $\boldsymbol{K}_1 = 8\boldsymbol{I}_{8\times 8}$. The gain matrix $\boldsymbol{K}_2$ of the BC is designed to be $\boldsymbol{K}_2 = 2\boldsymbol{I}_{8\times 8}$.

A. Stabilization problem

The initial coordinate of the quadrotor manipulator is denoted as $\boldsymbol{\xi}_{\mathrm{QM}}^0$, which is

$$\boldsymbol{\xi}_{\mathrm{QM}}^0 = \begin{bmatrix} 0 & 0 & -8 & 0 & 0 & 0 & \frac{3}{4}\pi & \frac{1}{2}\pi \end{bmatrix}^{\mathrm{T}}. \tag{39}$$

The desired coordinate of the quadrotor manipulator is denoted as $\boldsymbol{\xi}_{\mathrm{QM}}^{\mathrm{d}}$, which is assigned to be

$$\boldsymbol{\xi}_{\mathrm{QM}}^{\mathrm{d}} = \begin{bmatrix} 0.6 & 0.6 & -9 & \frac{1}{12}\pi & \frac{1}{12}\pi & \frac{1}{4}\pi & \frac{3}{5}\pi & \frac{2}{3}\pi \end{bmatrix}^{\mathrm{T}}. \tag{40}$$

The wind disturbance described in (37) is imposed on the quadrotor manipulator only from 0 to 12.5 s. The simulation of stabilization problem is divided into two cases. One case is for the system (11) under the control of the BC. The other case is for the system (11) controlled by the BSTSMC.

The position responses of the quadrotor are shown in Fig. 2. It is observed that the responses of the BSTSMC converge to desired positions more quickly than those of the BC. The settling time of the BSTSMC is about 1.7 s and the settling time of the BC is about 2.3 s. Due to the influence of the external wind disturbance, the position responses of the quadrotor under the control of the BC oscillate around the desired position in finite frequency and amplitude. When the external wind disturbance disappears from 12.5 s , the position responses of the BC converge soon to the desired positions. In contrast, no oscillations are observed for the

BSTSMC in the period with the external wind disturbance. After 1.7 s, the position responses of the BSTSMC can still follow closely the desired positions despite the external wind disturbance. Similar phenomena can also be observed in the orientation responses and the joint angle responses of the manipulator (see Fig. 3 and Fig. 4).

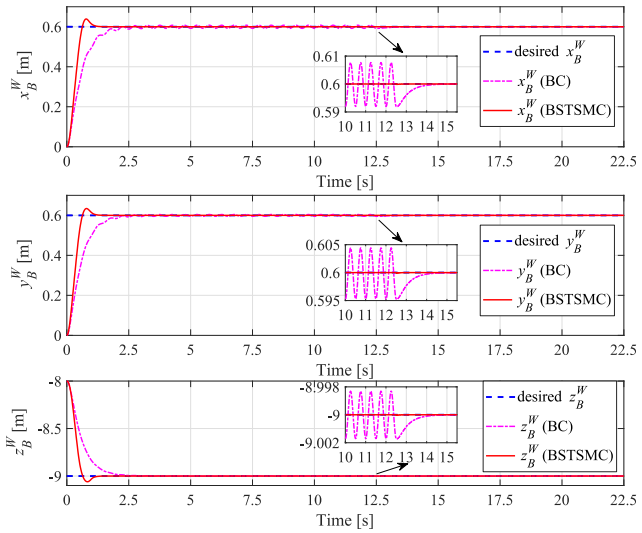

Fig. 2. Position responses of the quadrotor in the stabilization problem

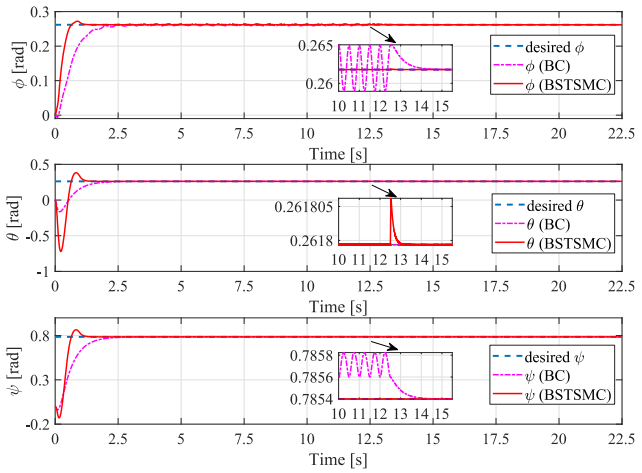

Fig. 3. Orientation responses of the quadrotor in the stabilization problem

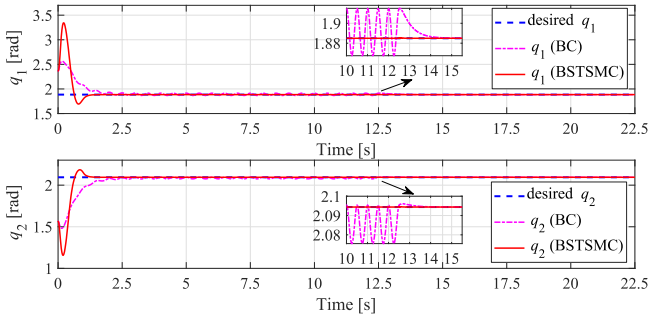

Fig. 4. Joint angles of the manipulator in the stabilization problem

It should be pointed out that internal interactions between the quadrotor and the manipulator will result in oscillations in the responses of the BC, even though there are no external disturbances exerted on the input channel of both the orientation of the quadrotor and the joint angles of the manipulator. As shown in Fig. 5 and Fig. 6, there is no obvious chattering excited by the BSTSMC in both the angular velocity and the tilting angle of each rotor, no matter the external wind disturbance exists or not. Also, no chattering phenomenon is found in the torque inputs of the manipulator, which is shown in Fig. 7.

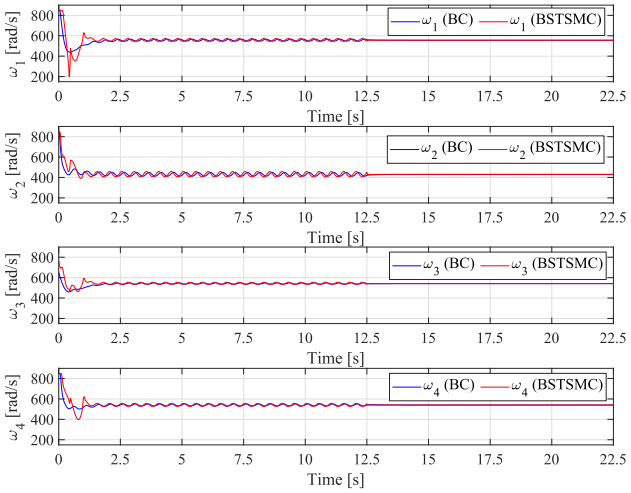

Fig. 5. Angular velocity of each rotor in the stabilization problem

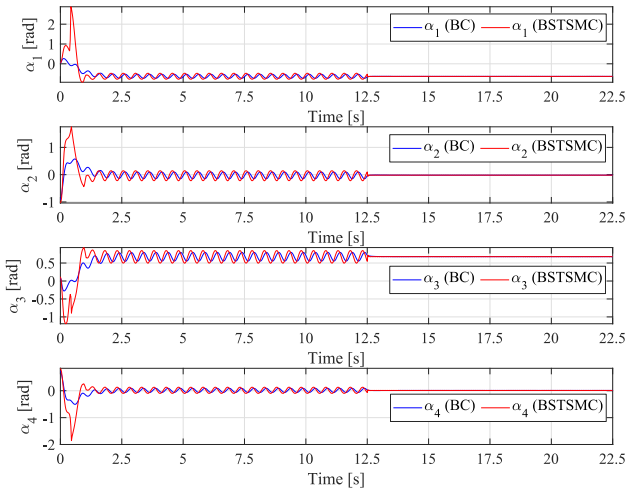

Fig. 6. Tilting angle of each rotor in the stabilization problem

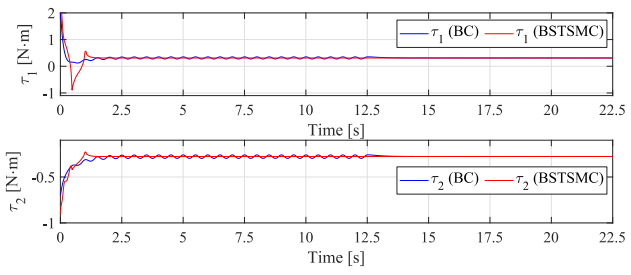

Fig. 7. Torque inputs of the manipulator in the stabilization problem

B. Trajectory tracking problem

The coordinate of the tip of the end-effector in the task space is defined as below:

$$\boldsymbol{\xi}_{\mathrm{e}} \triangleq [x_{\mathrm{e}} \quad y_{\mathrm{e}} \quad z_{\mathrm{e}} \quad \phi_{\mathrm{e}} \quad \theta_{\mathrm{e}} \quad \psi_{\mathrm{e}}]^{\mathrm{T}}, \tag{41}$$

Then, the generalized coordinates of the quadrotor manipulator $\boldsymbol{\xi}_{\mathrm{QM}}$ can be derived from $\boldsymbol{\xi}_{\mathrm{e}}$ based on Eq. (9) by numerical calculation.

The wind disturbance is exerted on the quadrotor manipulator in the period of 0 to 12.5 s. The initial coordinate of the quadrotor manipulator is chosen to be

$$\xi_{\mathrm{QM}}^{0}=\left[0.7 \quad 0 \quad -8.7 \quad 0 \quad 0 \quad 0 \quad \frac{3}{4}\pi \quad \frac{1}{2}\pi\right]^{\mathrm{T}}. \tag{42}$$

TABLE II. DESIRED TRAJECTORY OF THE END-EFFECTOR

x_{e} [m]	0.7	$0.7\cos\left(\frac{\pi}{5}t\right)$
y_{e} [m]	0	$0.7\sin\left(\frac{\pi}{5}t\right)$
z_{e}[m]	-8.5	$-8.5-0.2t$
ϕ_{e} [rad]	0	$\frac{\pi}{24}\sin\left(\frac{\pi}{5}(t-2.5)\right)$
θ_{e} [rad]	0	$\frac{\pi}{24}\sin\left(\frac{\pi}{5}(t-2.5)\right)$
ψ_{e} [rad]	0	$\frac{\pi}{5}\sin\left(\frac{\pi}{5}(t-2.5)\right)$
t [s]	[0,2.5)	[2.5,22.5]

The desired trajectory of the tip of the end-effector is a helix, which is shown in Fig. 8. Its details are shown in Table II. Both the BC and the BSTSMC are applied to the quadrotor manipulator system to evaluate and compare the performances of the two controllers.

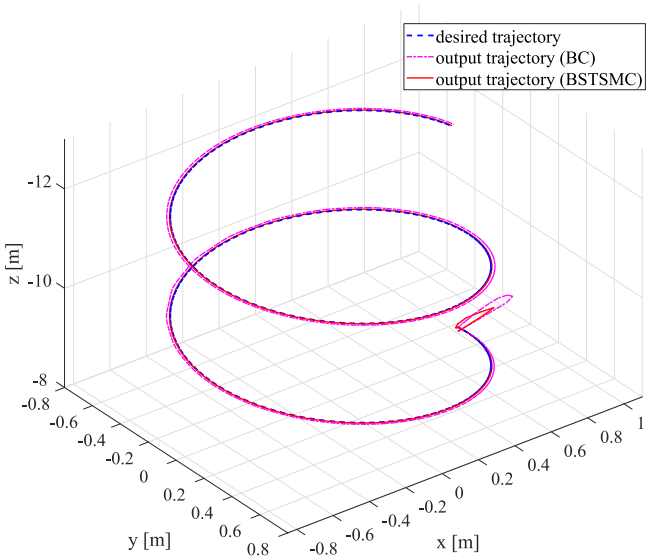

Fig. 8. Trajectory of the tip of the end-effector in 3D space

In the period of 0 to 2.5 s, the quadrotor manipulator is commanded to hover at the same position and to be prepared for the next helix trajectory tracking. The position, orientation and joint angle responses are shown in Fig. 9, Fig. 10 and Fig. 11, respectively. Apparently, the BSTSMC can suppress the influence of the external wind disturbance from 2.5 to 12.5 s, because the errors of the responses of the BSTMC are much smaller than those of the BC. In order to quantitatively evaluate the errors, the following root-mean-square (RMS) errors [39]-[41] are introduced:

$$\mathrm{RMS}(e_1(i))=\sqrt{\frac{1}{N}\sum_{i=1}^{N}(e_1(i))^2},\ i=1\ldots 8, \tag{43}$$

where $e_1(i)$ is the i th element of e_1 and N is the number of sampling steps in the simulation. RMS errors of each element of e_1 of both the BC and the BSTSMC are summarized in Table III. From Table III, it is obvious that the RMS errors of $\boldsymbol{e}_1$ of the BSTSMC under the influence of external wind disturbance is less than those of the BSTSMC with no external wind disturbance. The same conclusion can be achieved for the BC except for $e_1(2)$. Under the same circumstance (with external wind disturbance or not), the RMS errors of $\boldsymbol{e}_1$ of the BSTSMC is less than those of the BC.

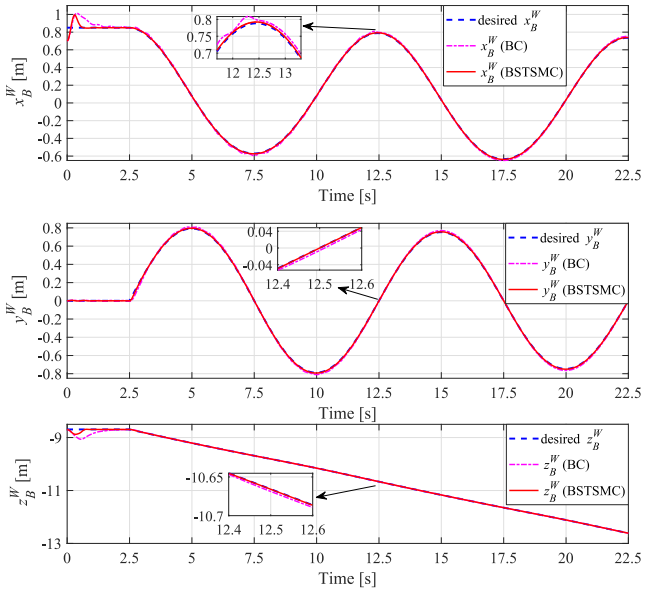

Fig. 9. Position responses of the quadrotor in the trajectory tracking problem

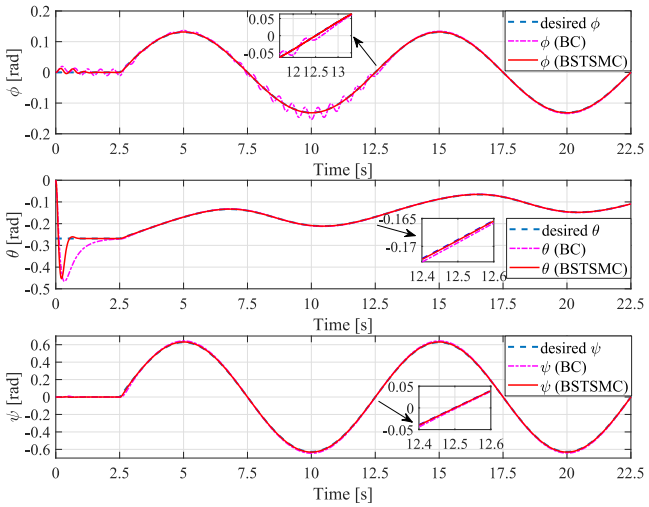

Fig. 10. Orientation responses of the quadrotor in the trajectory tracking problem

TABLE III. RMS ERRORS OF THE BC AND THE BSTSMC IN THE TRAJECTORY TRACKING PROBLEM

RMS errors	The BC (2.5 ~ 12.5 s)	The BC (12.5 ~ 22.5 s)	The BSTSMC (2.5 ~ 12.5 s)	The BSTSMC (12.5 ~ 22.5 s)
$e_1(1)$	1.223×10^{-2}	1.081×10^{-2}	2.366×10^{-3}	2.441×10^{-3}
$e_1(2)$	1.587×10^{-2}	1.232×10^{-2}	4.272×10^{-3}	2.638×10^{-3}
$e_1(3)$	3.734×10^{-3}	1.374×10^{-3}	1.351×10^{-3}	1.419×10^{-4}
$e_1(4)$	8.935×10^{-3}	2.990×10^{-3}	7.163×10^{-4}	4.592×10^{-4}
$e_1(5)$	1.454×10^{-3}	9.102×10^{-4}	3.346×10^{-4}	1.956×10^{-4}
$e_1(6)$	1.335×10^{-2}	1.030×10^{-2}	3.314×10^{-3}	2.199×10^{-3}
$e_1(7)$	3.041×10^{-2}	9.864×10^{-3}	1.168×10^{-3}	3.435×10^{-4}
$e_1(8)$	1.566×10^{-2}	3.680×10^{-3}	5.867×10^{-4}	2.190×10^{-4}

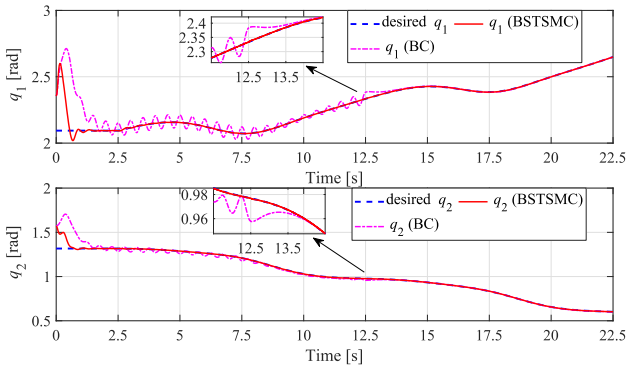

Fig. 11. Joint angles of the manipulator in the trajectory tracking problem

Despite the wind disturbances during 2.5 s to 12.5 s, the BSTSMC can still make sure the tip of the end-effector of the manipulator follow the trajectory closely (see Fig. 8). In contrast, the tip of the end-effector deviates from the desired trajectory when controlled by the BC. Even under the circumstance of no external wind disturbance, the performance of the BSTSMC is better than that of the BC. At the same time, no obvious chattering phenomenon is observed in the inputs (see Fig. 12, Fig. 13 and Fig. 14). Unlike the intense chattering phenomenon in the conventional sliding mode, the inputs generated by the BSTSMC is more friendly for the actuators to be implemented.

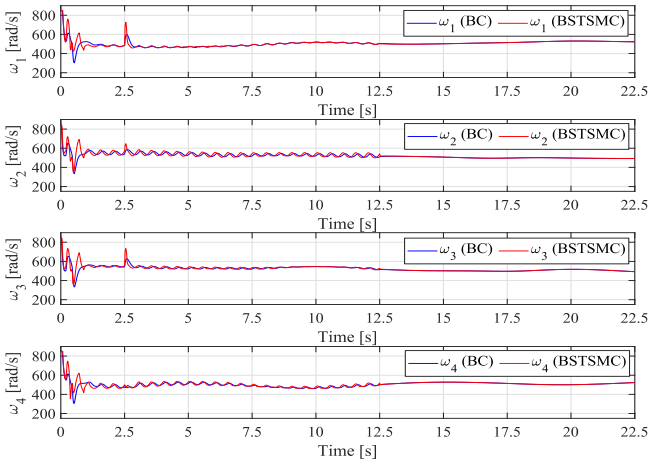

Fig. 12. Angular velocity of each rotor in the trajectory tracking problem

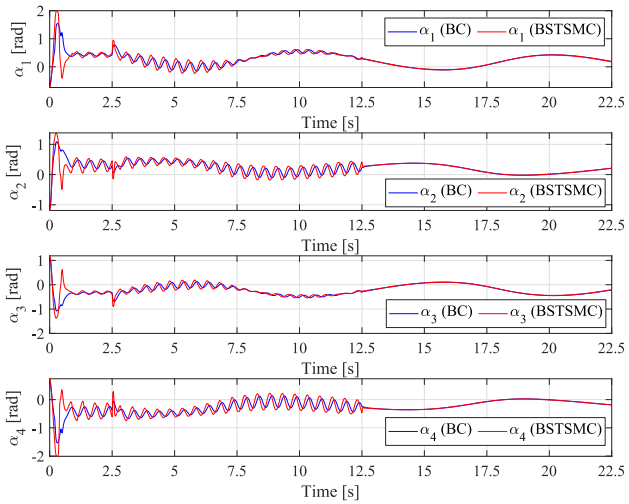

Fig. 13. Tilting angle of each rotor in the trajectory tracking problem

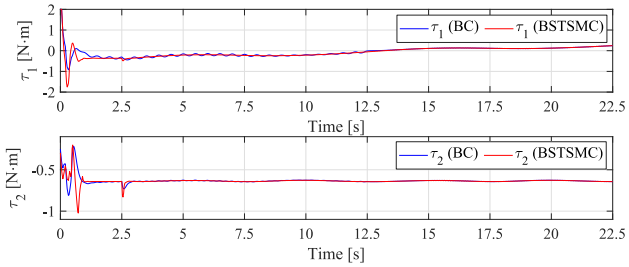

Fig. 14. Torque inputs of the manipulator in the trajectory tracking problem

C. Discussions

From the simulation results of stabilization problem and trajectory tracking problem, both the BSTSMC and the BC are capable of converging to reference. However, the BC is not robust enough to suppress the influence of external wind disturbance. The BSTSMC is proved to be a robust controller, which can reject the influence of the external disturbance. In terms of settling time in the stabilization problem and RMS errors in the trajectory tracking problem, the performance of the BSTSMC is superior to that of the BC.

V. CONCLUSIONS AND FUTURE WORKS

In this paper, a backstepping-based super-twisting sliding mode controller (BSTSMC) has been proposed to be applied

to the quadrotor manipulator with four tiltable rotors. The stability of the proposed was proved by applying the Lyapunov stability theory. The performance of the BSTSMC was validated by simulations with comparisons with the BC. The overall performance of the BSTSMC was superior to that of the BC. The property of the BSTSMC for attenuating a chattering phenomenon in the inputs was also checked and understood in the simulations. At the same time, the decoupling controlling of the position and the orientation of the quadrotor manipulator was verified. In this research, only external wind disturbances were considered. As one of the future works, payload variation should be considered in the practical application of the quadrotor manipulator. In addition to the robustness of the controller with respect to the external wind disturbances and parameter perturbations resulted from payload variation, it is very important to take the force control or the hybrid control of position and force into consideration for a task implemented by the quadrotor manipulator from the air.

REFERENCES

[1] X. Meng, Y. He, and J. Han, "Survey on aerial manipulator: System, modeling, and control," Robotica, vol. 38, no. 7, pp. 1288–1317, 2020.

[2] F. Ruggiero, M. Trujillo, R. Cano, H. Ascorbe, A. Viguria, C. Perez, V. Lippiello, A. Ollero, and B. Siciliano, "A multilayer control for multirotor uavs equipped with a servo robot arm," in 2015 IEEE International Conference on Robotics and Automation (ICRA), Seattle, WA, USA, May 26–30, 2015, pp. 4014–4020.

[3] F. Ruggiero, V. Lippiello, and A. Ollero, "Aerial manipulation: A literature review," IEEE Robotics and Automation Letters, vol. 3, no. 3, pp. 1957–1964, 2018.

[4] C. Kuchwa-Dube and J. O. Pedro, "Quadrotor-based aerial manipulator altitude and attitude tracking using adaptive super-twisting sliding mode control," in 2019 International Conference on Unmanned Aircraft Systems (ICUAS), Atlanta, GA, USA, June 11–14, 2019, pp. 144–151.

[5] F. Gramazio, T. Cadalbert, F. Augugliaro, M. Kohler, J. Willmann, and R. D'Andrea, "Aerial Robotic Construction Towards a New Field of Architectural Research," International Journal of Architectural Computing, vol. 10, no. 3, pp. 439–460, 2012.

[6] T. W. Danko and P. Y. Oh, "Design and control of a hyper-redundant manipulator for mobile manipulating unmanned aerial vehicles," Journal of Intelligent & Robotic Systems, vol. 73, no. 1, pp. 709–723, 2014.

[7] A. Suarez, A. E. Jimenez-Cano, V. M. Vega, G. Heredia, A. RodriguezCastano, and A. Ollero, "Design of a lightweight dual arm system for aerial manipulation," Mechatronics, vol. 50, pp. 30–44, 2018.

[8] A. Ollero, G. Heredia, A. Franchi, G. Antonelli, K. Kondak, A. Sanfeliu et al., "The aeroarms project: Aerial robots with advanced manipulation capabilities for inspection and maintenance," IEEE Robotics & Automation Magazine, vol. 25, no. 4, pp. 12–23, 2018.

[9] A. Mohiuddin, T. Tarek, Y. Zweiri, and D. Gan, "A Survey of Single and Multi-UAV Aerial Manipulation," Unmanned Systems, vol. 8, no. 2, pp. 119–147, 2020.

[10] A. Ollero, M. Tognon, A. Suarez, D. Lee, and A. Franchi, "Past, present, and future of aerial robotic manipulators," IEEE Transactions on Robotics, pp. 1–20, 2021, doi: 10.1109/TRO.2021.3084395.

[11] M. Fumagalli, R. Naldi, A. Macchelli, F. Forte, A. Q. Keemink, S. Stramigioli, R. Carloni, and L. Marconi, "Developing an aerial manipulator prototype: Physical interaction with the environment," IEEE robotics & automation magazine, vol. 21, no. 3, pp. 41–50, 2014.

[12] M. Fanni and A. Khalifa, "A new 6-dof quadrotor manipulation system: Design, kinematics, dynamics, and control," IEEE/ASME Transactions On Mechatronics, vol. 22, no. 3, pp. 1315–1326, 2017.

[13] G. Heredia, A. E. Jimenez-Cano, I. Sanchez, D. Llorente, V. Vega, J. Braga, J. A. Acosta, and A. Ollero, "Control of a multirotor outdoor aerial manipulator," in 2014 IEEE/RSJ International Conference on Intelligent Robots and Systems, Chicago, IL, USA, September 14–18, 2014, pp. 3417–3422.

[14] S. Rajappa, M. Ryll, H. H. Bulthoff, and A. Franchi, "Modeling, control and design optimization for a fully-actuated hexarotor aerial vehicle with tilted propellers," in 2015 IEEE international conference on robotics and automation (ICRA), Seattle, WA, USA, May 26–30, 2015, pp. 4006–4013.

[15] M. Ryll, G. Muscio, F. Pierri, E. Cataldi, G. Antonelli, F. Caccavale, and A. Franchi, "6d physical interaction with a fully actuated aerial robot," in 2017 IEEE International Conference on Robotics and Automation (ICRA), Singapore, Singapore, May 2017, pp. 5190–5195.

[16] P. J. Sanchez-Cuevas, A. Gonzalez-Morgado, N. Cortes, D. B. Gayango, A. E. Jimenez-Cano, A. Ollero, and G. Heredia, "Fully-actuated aerial manipulator for infrastructure contact inspection: Design, modeling, localization, and control," Sensors, vol. 20, no. 17, 2020, doi: 10.3390/s20174708.

[17] M. Ryll, D. Bicego, and A. Franchi, "Modeling and control of fast-hex: A fully-actuated by synchronized-tilting hexarotor," in 2016 IEEE/RSJ International Conference on Intelligent Robots and Systems (IROS), Daejeon, Korea, October 9–14, 2016, pp. 1689–1694.

[18] R. Rashad, J. Goerres, R. Aarts, J. B. Engelen, and S. Stramigioli, "Fully actuated multirotor uavs: A literature review," IEEE Robotics & Automation Magazine, vol. 27, no. 3, pp. 97–107, 2020.

[19] S. Waslander and C. Wang, "Wind disturbance estimation and rejection for quadrotor position control," in AIAA Infotech@ Aerospace conference and AIAA unmanned... Unlimited conference, Seattle, WA, USA, April 6–9, 2009, doi: 10.2514/6.2009-1983.

[20] P. Abichandani, D. Lobo, G. Ford, D. Bucci, and M. Kam, "Wind Measurement and Simulation Techniques in Multi-Rotor Small Unmanned Aerial Vehicles," IEEE Access, vol. 8, pp. 54 910–54 927, 2020.

[21] A. Suarez, G. Heredia, and A. Ollero, "Physical-virtual impedance control in ultralightweight and compliant dual-arm aerial manipulators," IEEE Robotics and Automation Letters, vol. 3, no. 3, pp. 2553–2560, 2018.

[22] Z. A. Ali and X. Li, "Modeling and controlling of quadrotor aerial vehicle equipped with a gripper," Measurement and Control, vol. 52, no. 5-6, pp. 577–587, 2019.

[23] R. Jiao, W. Chou, Y. Rong, and M. Dong, "Anti-disturbance control for quadrotor UAV manipulator attitude system based on fuzzy adaptive saturation super-twisting sliding mode observer," Applied Sciences, vol. 10, no. 11, 2020, doi: 10.3390/app10113719.

[24] Y. Shtessel, C. Edwards, L. Fridman, and A. Levant, Sliding mode control and observation. New York, NY, USA: Birkhauser, 2014, pp. 89–99.

[25] R. Coban, "Backstepping integral sliding mode control of an electromechanical system," Automatika, vol. 58, no. 3, pp. 266–272, 2017.

[26] Y. Shtessel, M. Taleb, and F. Plestan, "A novel adaptive-gain supertwisting sliding mode controller: Methodology and application," Automatica, vol. 48, no. 5, pp. 759–769, 2012.

[27] H. Lee and V. I. Utkin, "Chattering suppression methods in sliding mode control systems," Annual reviews in control, vol. 31, no. 2, pp. 179–188, 2007.

[28] V. Utkin and J. Shi, "Integral sliding mode in systems operating under uncertainty conditions," in Proceedings of 35th IEEE Conference on Decision and Control, vol. 4, Kobe, Japan, December 1996, pp. 4591–4596.

[29] V. Utkin, "On convergence time and disturbance rejection of supertwisting control," IEEE Transactions on Automatic Control, vol. 58, no. 8, pp. 2013–2017, 2013.

[30] J. Davila, L. Fridman, and A. Levant, "Second-order sliding-mode observer for mechanical systems," IEEE transactions on automatic control, vol. 50, no. 11, pp. 1785–1789, 2005.

[31] A. Levant, "Sliding order and sliding accuracy in sliding mode control," International journal of control, vol. 58, no. 6, pp. 1247–1263, 1993.

[32] Y. Kali, M. Saad, and K. Benjelloun, "Backstepping super-twisting for robotic manipulators with matched and unmatched uncertainties," in 2021 18th International Multi-Conference on Systems, Signals & Devices (SSD), Monastir, Tunisia, March 22–25, 2021, pp. 1154–1159.

[33] T. Huynh and Y. Kim, "A study on gimbal motion control system design based on super-twisting control method," Journal of the Korean Society for Precision Engineering, vol. 38, no. 2, pp. 115–122, 2021.

[34] S. Yi, K. Watanabe, and I. Nagai, "Anti-disturbance control of a quadrotor manipulator with tiltable rotors based on integral sliding mode control," Artificial Life and Robotics, vol. 26, pp. 513—-522, 2021, doi: 10.1007/s10015-021-00700-3.

[35] S. R. Buss, "Introduction to Inverse Kinematics with Jacobian Transpose, Pseudoinverse and Damped Least Squares methods," Department of Mathematics University of California, San Diego, CA, Tech. Rep., 2009.

[36] H. M. M. Adil, S. Ahmed, and I. Ahmad, "Control of MagLev System Using Supertwisting and Integral Backstepping Sliding Mode Algorithm," IEEE Access, vol. 8, pp. 51 352–51 362, 2020.

[37] M. Basin, C. B. Panathula, and Y. Shtessel, "Multivariable continuous fixed-time second-order sliding mode control: design and convergence time estimation," IET Control Theory & Applications, vol. 11, no. 8, pp. 1104–1111, 2017.

[38] I. Nagesh and C. Edwards, "A multivariable super-twisting sliding mode approach," Automatica, vol. 50, no. 3, pp. 984–988, 2014.

[39] G. M. Bone and S. Ning, "Experimental comparison of position tracking control algorithms for pneumatic cylinder actuators," IEEE/ASME Transactions on mechatronics, vol. 12, no. 5, pp. 557–561, 2007.

[40] S. Yin and B. Xiao, "Tracking control of surface ships with disturbance and uncertainties rejection capability," IEEE/ASME transactions on mechatronics, vol. 22, no. 3, pp. 1154–1162, 2016.

[41] J. Guerrero, J. Torres, E. Antonio, and E. Campos, "Autonomous underwater vehicle robust path tracking: Generalized super-twisting algorithm and block backstepping controllers," Journal of Control Engineering and Applied Informatics, vol. 20, no. 2, pp. 51–63, 2018.